Surrogate-model based Optimization Framework for the Structural Design of Helicopter Rotor Blades subject to Dynamics and Failure Criteria

Rohin Kumar Majeti
Research Scientist
Institute of Flight Systems

Franziska Becker
Research Scientist
Institute of Lightweight Systems

German Aerospace Center (DLR)
Braunschweig, Germany

ABSTRACT

Helicopter rotor hub vibratory loads can be alleviated through careful design of the rotor blade inner structure. Large design space and the nonlinear nature of the problem are major obstacles that need to be overcome. Apart from that, the need for high-fidelity solutions lead to high computational times. An automated surrogate-model based design optimization process using commercially available software as well as codes developed within DLR has been described in this paper. Minimal human interference and overall process efficiency is the goal of this work. Latin Hypercube Sampling function for the design of experiments, Kriging function for surrogate modeling and particle swarm optimization algorithm make up the framework. The rotor blade inner structure parameters constitute the design variables while the natural frequencies and vibration index are taken as objective functions. Results show that through careful design of the inner structure, it is possible to obtain a rotor with lower hub vibratory loads. For the optimization process, it must be ensured that sufficient number of sampling points are taken for building accurate surrogate models and the problem definition should be neither under-constrained nor over-constrained.

NOTATION

AI	Autorotation index, m
cg, CG	Center of gravity
sc, SC	Shear center
ac, AC	Aerodynamic center
es	Offset of cg axis to elastic axis, m
e0	Offset of elastic axis and the pitch axis at the blade root, m
f	Objective function for optimization
F1, F2, F3	First three flap modes
L1, L2	First two lag modes
T1	First torsional mode
F_{4x}, F_{4y}, F_{4z}	Rotor hub 4/rev forces, N
M_{4x}, M_{4y}, M_{4z}	Rotor hub 4/rev moments, Nm
I_R	Polar moment of inertia of rotor about its shaft,
r	radial location parameter, m
R	Radius of the rotor, m
T	Required thrust specified for the rotor, N
VI	Vibration index
$w_1,\ldots w_6$	weighting factors for frequencies
w_F, w_M	weighting factors for hub forces, moments
W	Gross weight of the helicopter, N
z	Flap tip deflection / R
ω	Rotor blade natural frequency, rad/s
Ω	Rotor rotational frequency, rad/s
DOE	Design of Experiments
PSO	Particle swarm optimization

INTRODUCTION

Helicopter rotor design is a challenging task given the wide scope of objectives it needs to fulfill. Performance, vibrations, noise, stability, weight minimization, structural strength limits are only some of the multiple factors a designer has to consider. In addition, the couplings among structures, dynamics and aerodynamics components of the rotor blade

Presented at the Vertical Flight Society's 79th Annual Forum & Technology Display, West Palm Beach, FL, USA, May 16-18, 2023.

make its design a complex multidisciplinary process. Rotor blade design consists of two parts –

1) external shape design dealing with the planform, twist and airfoil selection which are mainly driven by aerodynamics (Ref.s 1, 2);
2) internal structural design dealing with the structural components propping up the airfoil (Ref. 3).

Rotor blades being aeroelastic in nature, both parts of the design are equally important. The multidisciplinary nature of rotor design makes it an appropriate candidate for optimization methods. Application of formal methods of optimization to rotor blades started in the 1980s. In his review of the eighties and early nineties trends in rotor system design in Ref. 4, the author refers to "aeroelastic optimization" which is the optimum selection of structural, inertial and aerodynamic characteristics of the blades to minimize helicopter vibrations. A systematic sensitivity study to examine the influence of blade stiffness, spanwise mass distribution, chordwise location of blade center of gravity, twist, tip sweep and airfoil camber on oscillatory hub loads of a four-bladed articulated rotor was carried out in Ref. 5. An optimization technique to obtain optimum rotating natural frequencies and minimum blade weight by distributions of mass and stiffness properties of rotor blades and constraining the flap inertia is described in Ref. 6. In Ref. 7, a survey of researches focusing on the progress in rotorcraft design optimization in the late nineties and early 2000's was published. In Ref. 8, composite ply angles were designed to minimize the vibratory hub loads subject to certain constraints. Failure analysis in a design optimization process of a composite rotor blade was considered in Ref. 9.

Composite materials have high strength-to-weight ratio and superior fatigue properties when compared to metals and hence, have been preferred for rotor blades. However, for the designer, composites complicate and increase the cost of the optimization process because of the large number of design variables they introduce. To reduce complexity, it is quite the norm to assume the topology of structural components inside the cross-section of the blade and vary their dimensions and locations, thus converting the problem to that of a sizing optimization (Ref. 10). For instance, in (Ref. 11), the layout of the cross-section is fixed with a D-spar. The thickness of the D-spar, skin and back of spar along with spar location and orientation were considered as variables with the objective being minimization of the distance between the shear center and the quarter-chord.

The design space for rotors are often non-convex and can have multiple local minima. Gradient-based optimization algorithms can get stuck at a local minimum point (Ref. 12). Non-gradient methods like genetic algorithms (GA) and particle swarm optimization (PSO) have proven invaluable because of their ability in finding global minima and permitting the use of discrete design variables (Ref. 13). For multiple evaluations of the objective functions in the course of optimization, the computationally expensive high-fidelity comprehensive analyses needed for performance, vibrations and loads calculations can be prohibitive. An approximation concept like the surrogate-model based design optimization is an efficient way to reduce computational cost (Ref. 14). In Ref. 15, objective functions evaluated in a Design of Experiments were used to build response surface models which were then used in a Monte Carlo simulation to identify a Pareto optimum. In order to overcome the perceived limitations of the conventional surrogate models to represent the nonlinearity of aeroelastic responses of the rotor, an improved surrogate model using machine learning techniques – Cluster Kriging – was used in Ref. 16 resulting in higher vibration reduction than that achieved using single Kriging.

Automation is a given for multidisciplinary optimization. In line with the industry preference for off-the-shelf detailed analysis capability, the current work aims to improve upon current design methods by setting up an automated surrogate-model based design optimization process using commercially

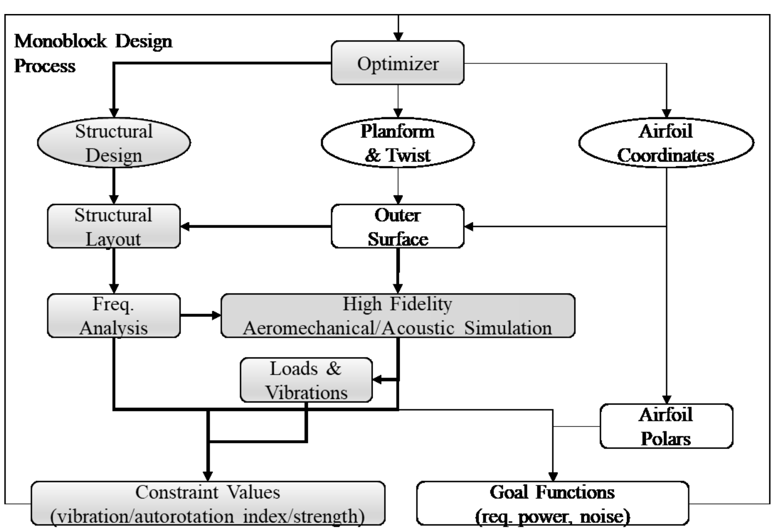

Figure 1. Multidisciplinary rotor blade optimization process

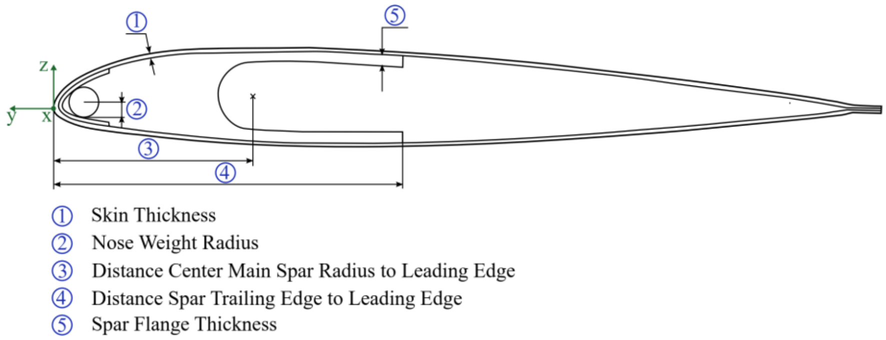

Figure 2. Rotor blade cross-sectional inner structure

available software as well as computer codes developed within DLR. Minimal human interference is intended in order to reduce the design time and to improve overall efficiency. For instance, parametric and feature-based models facilitate automatic model changes. Such a design process reduces development time and costs.

HELICOPTER ROTOR BLADE DESIGN

The DLR internal project URBAN-Rescue envisions two concepts: a high-speed rescue helicopter with noise-reducing rotor and fixed wings, and a small medical-transporter in the mode of an urban air mobility (UAM) multicopter. The aim of one of the work packages of URBAN-Rescue is to combine the individual sub-processes of the various institutes involved in rotor blade design into a formal overall process. Within this scope, performance and acoustics are the major drivers of the design with structural strength and dynamic behavior forming the boundary conditions. Computational cost and development times, being important practical factors, the project also endeavors to reduce them through automation and through surrogate modeling. Figure 1 shows a schematic of the overall rotor blade design process. For the purpose of the current project, only optimization of the airfoiled section of the blade is considered. The root section, which has a major influence on the first frequencies of hingeless and bearingless rotors, was left untouched for the current exercise.

This paper concerns only the internal structural design aspect of this process while the aerodynamics aspects of the project are similar to those described in Ref.s 17, 18. The optimization process for the structural side of the process is shaded in Fig. 1. On the aerodynamics side, performance and aero-acoustic optimization are carried out considering independent flight conditions like hover, cruise and descent. A multi-objective design approach coupled with surrogate models is utilized to find a Pareto optimal set of rotors. The utilization of the Pareto front approach is necessary to find good rotor designs, while CFD optimized blades were found to lead to more robust designs. A similar systematic optimization process is to be followed on the structural side of the design process.

Vibration Reduction

One of the major concerns in the design of rotor blades is to keep the vibratory hub loads to a minimum. In the case of a rotor with 4 identical blades, the (3/4/5)/rev blade loads in the rotating frame generate 4/rev hub loads in the fixed frame which are then transferred to the fuselage. This, being the first blade passage harmonic, is also the most important one. Blades have to be designed such that they are not generating high (N-1), N, (N+1)/rev blade loads, where N is the number of blades in the rotor.

One of the ways this can be achieved is by increasing the separation of blade natural frequencies from multiples of nominal rotational frequency and from the forcing frequencies which produce fuselage vibrations. Similarly, spanwise and chordwise distributions of blade mass can be chosen to minimize vibratory root shears. Vibrations may be reduced by inducing torsional motion which decreases angle of attack oscillations through the use of lumped masses. For example, chordwise offset of the center of gravity (cg) and aerodynamic center (ac) can be expected to produce coupling between torsional and flapwise bending response. If the torsional response is phased properly, it can produce an opposing airload to that produced by inflow. The net effect can be reduced root loads. Significant vibration reductions can be derived by placing the blade section cg forward of the aerodynamic center. Placing the cg at the quarter-chord or slightly forward of it is recommended for pitch-flap stability of the blade.

Lumped masses are also added at certain radial locations in order to reduce the hub vibrations. As seen in Ref. 19, simultaneous changes in the mode shapes and airloads due to the lumped masses result in a reduction of the generalized force and subsequently the hub shear. The underlying mechanism of vibration reduction also includes the interplay between inertia and centrifugal forces as a function of the radial location and magnitude of the masses. Typically, these masses are added at anti-nodes of the mode shape of the corresponding frequency which needs to be controlled.

Structural Design Chain at DLR

Prior to the URBAN-Rescue project, the structural layout and rotor dynamics tasks were decoupled and independently carried out. This meant manual exchange of information resulting in process inefficiency and fewer design iterations. A novelty of the URBAN-Rescue project is the integration of rotor dynamics into the structural layout optimization loop raising the potential for a smoother, automated and accelerated structural design process.

A typical rotor blade cross-sectional inner structure is shown in Fig. 2. In the simplest form, it consists of a skin with uniform thickness, a C-spar, and a foam core. A nose-weight is added to adjust the mass center offset with respect to the aerodynamic center. The C-spar is the main strength element of the inner structure. Its geometry is defined by the location of its center and the flange thickness & length. Freezing the size and weight of the spar, usually, requires quite a few design iterations. The C-spar is efficient in terms of material usage as compared to a D-spar. Another advantage of the C-spar is its ease of manufacture.

Given the rotor planform, twist and airfoil details as output from the aerodynamic optimization process, the design of internal structural components begins. The software suite used in the rotor design process include CATIA for CAD, ANSYS for FEA, SaMaRA (Ref. 20) for cross-sectional properties calculation and S4 (Ref. 21) for rotor aeromechanics. This way the three-dimensional beam analysis is decomposed into two-dimensional cross-sectional analysis and one-dimensional beam analysis. The structural modeling process is controlled and executed by a Python code. This contains the model generation structure as well as the interfacing between the submodules. The existing procedure for rotor blade model building has the following steps as can be seen from Fig. 3 –

1. The aerodynamic optimization delivers the outer geometry details of the blade in the form of point coordinates of the individual cross sections.
2. From this outer geometry details and a predefined cross-section topology template, the CAD models of several cross-sections of the rotor blade are built and extruded (Fig. 2). For a uniform blade, one cross-section is sufficient.
3. The Finite Element (FE) models of these cross-sections are then created.
4. These cross-sectional FE models are then adapted according to calculation requirements of the inhouse tool SaMaRA for calculation of cross-sectional properties.
5. Once the cross-sectional properties for the complete rotor blade are derived, they are then input to the inhouse rotor structural dynamics tool S4-FEM to perform modal analysis and extract natural frequencies.
6. The modal information is then fed to S4 which performs the trim analysis and outputs the hub loads and its harmonics.

CPACS (Common Parametric Aircraft Configuration Scheme, Ref. 22), developed at DLR for enabling the description and characterization of aircrafts, including rotorcraft, in XML-format, is used as the data exchange interface between the various software.

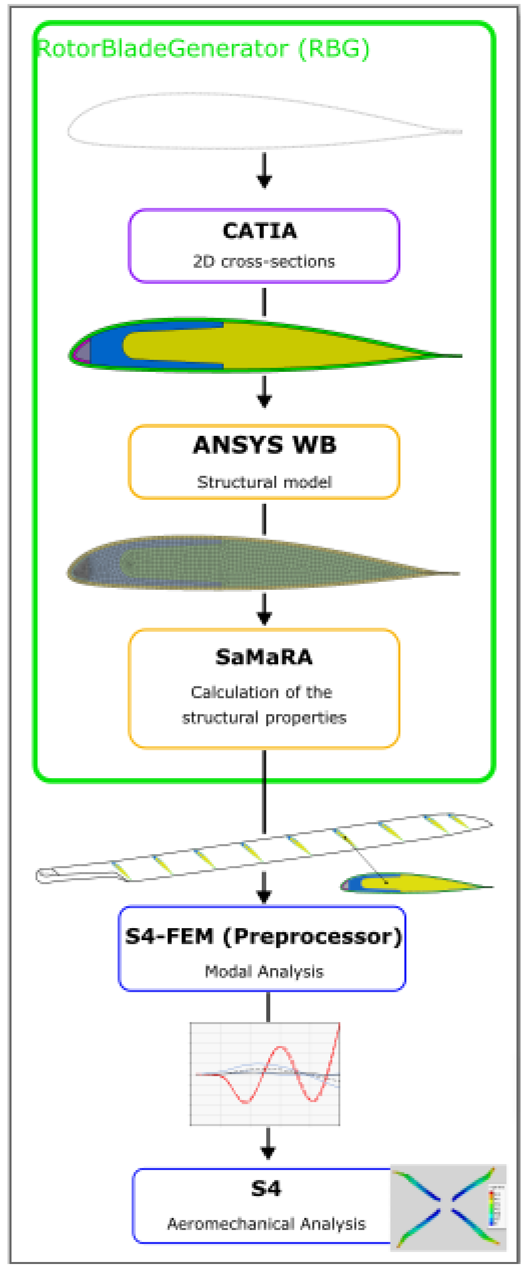

Figure 3. Rotor blade cross-sectional design chain

SURROGATE-BASED OPTIMIZATION

The design process described above is a time-consuming one and can take several days to find an acceptable solution for a variable section rotor blade even when automated. Optimization techniques reduce the workload of obtaining the optimum design from the designer. The optimization framework proposed in the current paper includes the automated design process along with a surrogate-based approach in combination with the non-gradient algorithm of

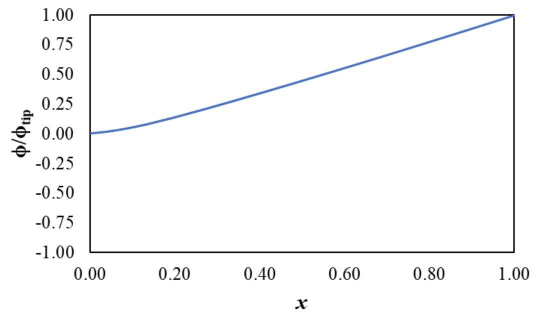

a. First flap mode shape

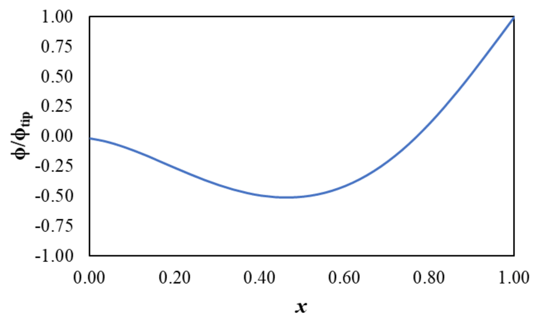

b. Second flap mode shape

Figure 4. Flap mode shapes of the baseline blade

Particle Swarm Optimization (PSO). Surrogate-based optimization techniques have been used earlier for the design of the composite rotor blade including in the aerodynamics part of the current project. An overview of the intended process is given in Fig. 5.

Design Variables

The five design parameters shown in Fig. 2 are selected as the variables for optimization. This then categorizes the problem to one of sizing optimization since the topology of structural components inside the given airfoil is assumed. The five parameters are skin thickness, radius of the nose weight, distance of the center of the main spar inner arc from the leading edge, distance of the trailing edge of the main spar flange from the leading edge and the spar flange thickness. Two lumped masses are added to the blade on the elastic axis – one at the tip (x=1.0) and one at the anti-node of the second flap mode of the baseline blade which is at about x=0.46 (Fig. 4b). Here *x*=0 is, normally, located at the virtual hinge or at the connection of the blade to the rotor head. The tip mass controls the first mode frequencies while the anti-node mass controls the second flap mode with less impact on the other modes. The second flap frequency, being close to 3/rev at the nominal design speed can be a major factor in hub vibrations since the blade 3/rev harmonics feed into the 4/rev hub harmonics. The magnitudes of these lumped masses are also taken as design variables bringing the total number to 7.

To limit the design space, upper and lower bounds are defined with regard to the design variables. Restrictions on the implementation of a successful structural model structure result from the functions used in the structure of the CAD geometry, the relationship between the respective parameters themselves and the mesh generation. In order to minimize the number of failed structural model generation, it is first defined to comply with functional restrictions with regard to the CAD model for each design variable upper and lower bound. In addition, known mesh sizing limits are considered as well. Considering dependency between the parameters themselves, a hierarchy of the dynamic parameter movement is determined. For example, the parameter skin thickness acts on the upper bound of the length of the spar flange, which means that the latter, if necessary, is reduced accordingly. In this way, the dependency in the parameter movement is taken into account and the lower and upper bounds dynamically applied to the parameter constellation chosen by the optimizer before the structure model generation begins. For the lumped masses, their magnitudes are limited such that the local blade mass density doesn't increase by more than 20% so that the overall blade mass increase is limited.

Design of Experiments (DOE)

In order to form the surrogate, the objective function must first be evaluated over an initial set of design points. The surrogate is then generated by interpolating the initial design points. The Latin hypercube sampling (LHS) function (Ref. 23) was used to generate the space-filling design of experiments used in this study. The points in the Latin hypercube represent the design points at which dynamic/aeroelastic simulations are to be conducted. Each simulation is independent of the simulations at other design points; therefore, the initial set of sample points can also be generated using distributed computers, if required.

Surrogate Modeling

Once an initial set of fitting points have been produced, surrogate models are created for the objective function and for the constraints. Surrogate models can be parametric or non-parametric. Kriging interpolation and Neural Networks are strong candidates for surrogate modeling (Ref. 24). Neural Networks are more suitable for highly nonlinear or very large problems and the computational expense can be high with it often requiring more than 10,000 training data points. Kriging is generally accepted as being a very effective method to approximate values over a design space (Ref.s 14, 18). Nevertheless, in order to examine how well the two models capture the nonlinearity of design space, they were tested for a test function of the form given in eq. 1 and having both polynomial and trigonometric nonlinear terms.

$$\mathbf{f = a_0 + a_1{*}x + a_2{*}y + a_{12}{*}x{*}y + a_{11}{*}x^2 + a_{22}{*}y^2 + a_s{*}\sin(x) + a_c{*}\cos(y)} \quad \mathbf{(1)}$$

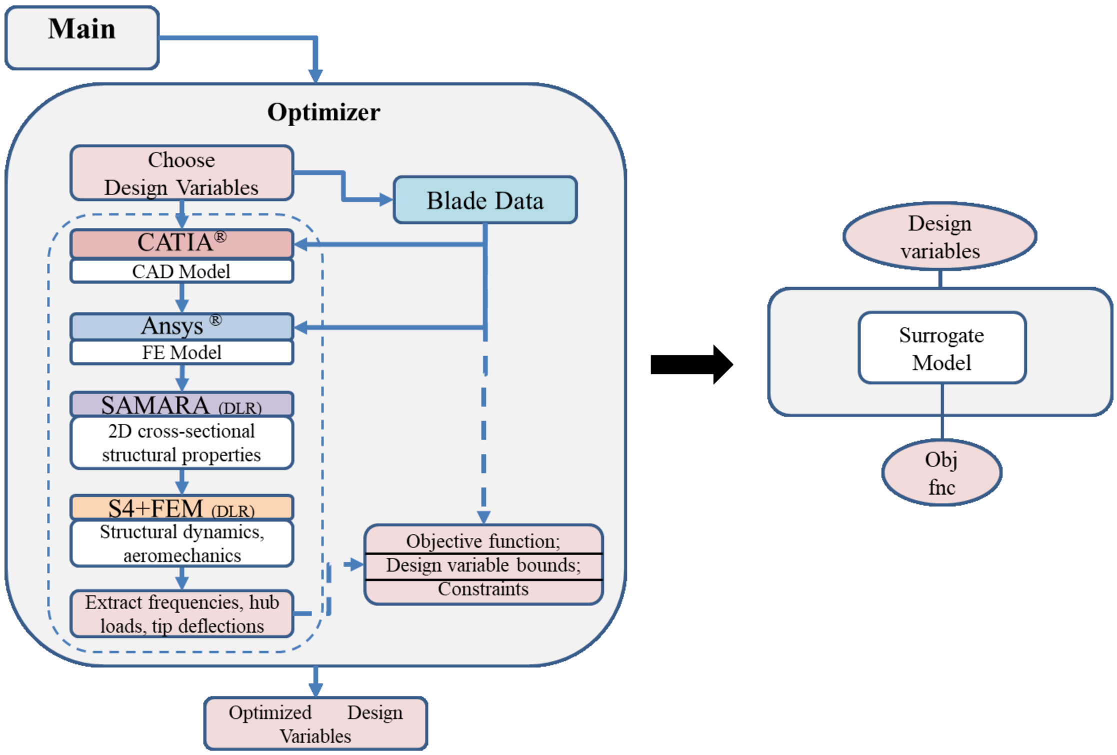

Figure 5. Flowchart of the rotor blade design optimization process

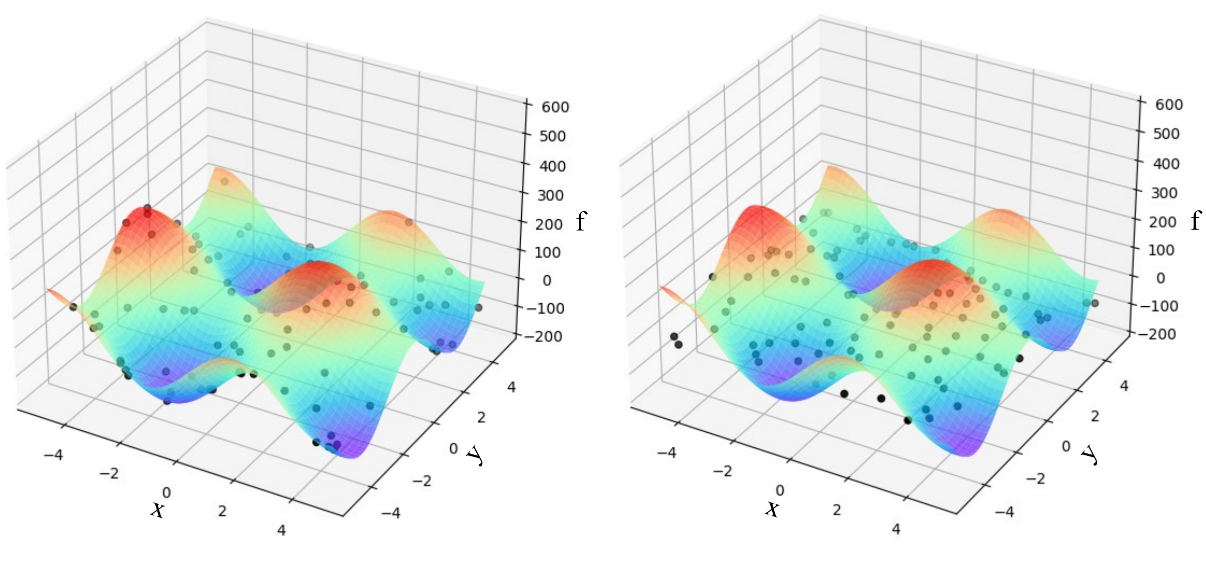

Figure 6. Surrogate model fit for test function

100 samples were used for the LHS DOE. The results are shown as 3D plots in Fig. 6. The design space is shown with actual function plotted as a surface and the predicted values from the surrogate model as dots. As can be seen the Kriging function gives a better approximation of the nonlinear function in this low-order problem than the gradient-enhanced neural network model. Based on the result of this simple test, Kriging has been chosen as the surrogate model for the current optimization problem.

Optimization Problem

It is intended to test out the newly developed optimization loop in incremental steps of complexity. Hence, to begin with, the HART II rotor blade (Ref. 21) which has a uniform section throughout the span is chosen as the baseline. While the final cross-sectional properties of the baseline blade are available, other details including the structural component sizing and information about materials used were not available. As a first step, a blade with an equivalent cross-section which has dynamic behavior as close as possible to the baseline blade is derived. The dynamics of the blade may be tuned with the help of lumped masses placed strategically along the span of the blade. The next step would be to achieve a configuration which can realize minimum vibration at the hub, reducing as much as possible from the baseline. This is achieved by ensuring that the natural frequencies are well separated from the operating frequency and its multiples. For the dynamic behavior problem, optimization was defined with a simple objective function, namely the root-mean-square deviation of the first six frequencies from those of the baseline blade. While the problem could be defined as multi-objective one, for simplicity the objectives are combined into a single function as follows -

Objective function for dynamic behaviour:

$$\boldsymbol{f} = \sqrt{\begin{array}{c}(w_1(\omega_{F1b} - \omega_{F1})^2 + w_2(\omega_{F2b} - \omega_{F2})^2 + \\ w_3(\omega_{F3b} - \omega_{F3})^2 + w_4(\omega_{L1b} - \omega_{L1})^2 + \\ w_5(\omega_{L2b} - \omega_{L2})^2 + w_6(\omega_{T1b} - \omega_{T1})^2)\end{array}} \tag{2}$$

Subscript ‘b’ in eq. 2 denotes baseline blade.

For the hub vibration problem, the vibration index (Ref.s 8, 14, 16) defined as follows was taken as the objective function

Objective function for hub vibration:

$$\boldsymbol{f} = w_F\sqrt{(F_{4x})^2 + (F_{4y})^2 + (F_{4z})^2} + w_M\sqrt{(M_{4x})^2 + (M_{4y})^2 + (M_{4z})^2} \tag{3}$$

In the above equation, the forces are nondimensionalized by the required thrust (T) and the moments are nondimensionalized by R*T. The vibration index value for the baseline rotor is used as a normalizing factor which means that if a rotor has vibration index less than 1, it has better vibratory characteristics than the baseline.

Design Constraints: The optimization is subject to the following constraints:

1. The first six natural frequencies of the blade are placed away from integer multiples of the rotor operational speed by at least 0.1/rev.
2. To reduce the dynamic coupling of bending and torsional loads, the offset between shear center and center of gravity is to be maintained equal to or less than 5% of chord length.
3. Similarly, the offset between the center of gravity and aerodynamic center (or quarter chord) is to be maintained equal to or less than 5% of the chord length with the center of gravity, preferably, forward.
4. Total mass of the optimized blade is to be maintained within 10% range of that of the baseline blade.
5. Since reduction in blade weights decrease rotational inertia, it has to be ensured that the autorotation index (Ref. 25) doesn’t reduce to less than 90% of the value for the baseline.

$$\boldsymbol{AI} = \frac{I_R\Omega^2}{2W}$$

6. In order to ensure the safety of the structure, tip deflection of the blade is limited to a value determined from the Tsai-Wu criterion (Ref. 26) for the baseline. The baseline blade is loaded till failure occurs as per this criterion. The corresponding tip flap deflection was about 0.04R.

Optimization Algorithm: Many of the classical optimization strategies require gradient information to determine the direction of the global optimum. However, these strategies are met with problems when there are multiple local minima. Evolutionary methods of optimization, on the other hand, require only the functional values and not the gradients. Due to their population approach, evolutionary methods can find multiple optimal solutions in a single simulation run and are thus, very suited for solving multi-objective optimization problems. Examples of popular evolutionary algorithms (EA) include Genetic algorithm, Differential Evolution, Particle Swarm Optimization etc.

Keeping long-term interests and scalability in mind, an EA - Particle swarm optimization (PSO) - was chosen as the algorithm for the initial trials of the new rotor design optimization process. PSO is an evolutionary algorithm based on the behavior of a colony of living organisms such as a flock of birds (Ref. 27). The method does not require gradients and can find global optima based on randomized start points and the knowledge of the current global and personal minima through its iterative, population-based character. This makes it suitable for running iterative and computationally expensive numeric programs.

In this method, a swarm of particles (population) is, initially, randomly distributed across the design space. The current position of each particle in the swarm at any point in time is

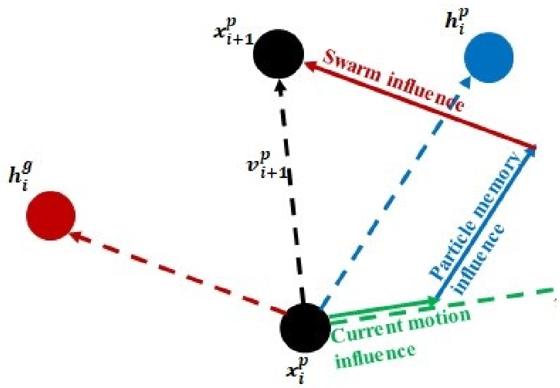

Figure 7. Position and velocity update for a swarm particle

then updated using a velocity vector. A unit time step is used ($\Delta t = 1$) here. The equations are illustrated in Fig. 7.

$$x^p_{i+1} = x^p_i + v^p_{i+1}\Delta t \quad \textbf{(4)}$$

$$v^p_{i+1} = wv^p_i + c_1 r_1 \frac{(h^p_i - x^p_i)}{\Delta t} + c_2 r_2 \frac{(h^g_i - x^p_i)}{\Delta t} \quad \textbf{(5)}$$

Here, x^p_i and v^p_i are the position and velocity of particle p at iteration i while x^p_{i+1} and v^p_{i+1} are the values at iteration $i+1$ which is away from i by Δt; r_1 and r_2 are randomly generated factors ranging from 0 to 1, which differ for each particle and iteration; h_i^p represents the best ever position of particle p where the objective function value is minimum, and h_i^g corresponds to the global best position up to iteration i for the minimal value of the objective function for the whole swarm. w, c_1 and c_2 are optimization parameters limited to the 0-1 range. w is the inertia weight controlling the exploring abilities of the swarm. Large inertia weights allow for global exploration of the design space. c_1 and c_2 are trust parameters indicating, respectively, how much confidence the current particle has in itself and how much in the swarm.

RESULTS

As already mentioned, the HART II rotor which is a scaled version of the BO-105 rotor has been used as the baseline for this work. The rotor operating condition detailed in Ref. 21 is used as the reference. The rotor blade geometry and the operating conditions which simulate a forward descent condition are summarized in Table 1. The optimization framework which was built was applied in a stepwise manner. A 600 sample LHS function was used with the seven parameters as the design variables. The complete design chain was run for the sample points of which 364 points resulted in successful runs. The failed cases were discarded and surrogate models were created for the objective functions (eq. 2 and 3)

Table 1. Rotor blade geometry and operating conditions

Characteristic	Value
Rotor geometry	
Rotor radius, m	2
Blade chord, m	0.121
Number of blades	4
Linear twist per span, deg	-8
Rotor solidity	0.077
Precone, deg	2.5
Airfoil	NACA23012 (trailing edge tab)
Rotor type	Hingeless
Operating conditions	
Rotational speed, rad/s	109.12
Rotor shaft angle of attack, deg	4.5
Advance ratio	0.151
Rotor thrust, N	3300
Rolling moment, Nm	20
Pitching moment, Nm	-20

and constraints from the successful cases. Optimization is then performed varying the objectives and constraints as described in the sections below.

Targeting same dynamic characteristics as baseline

In order to get the inner structure sizing which has the closest dynamic characteristics as the baseline blade, only eq. 1 is used as the objective. Lumped masses were not considered for this exercise. Among the constraints, the tip deflection one was left out because a complete aeromechanical analysis was not carried out; rather only dynamic analysis was performed to obtain the objective function (eq. 2).

PSO was used to search the design space for optimum objective function. Strict implementation of the constraints yielded no results, subsequent to which the constraints were relaxed. The frequency offset limit from multiples of rotor operational speed was removed for the third flap frequency because this mode is aerodynamically damped. Following this, two cases were considered – one having no restriction on the second lag frequency offset (I) and another having no restriction on the total mass of the blade (II).

The resulting inner structure profiles and the values of the variables are shown in Fig. 8 and Table 2. The difference in the inner structure profiles between the results and the baseline could be due to the consideration of only five of the design parameters out of many others within the optimization.

Table 2. Dimensions of the inner stucture

	Design variable	Iter I (mm)	Iter II (mm)
1	Skin thickness	0.44	0.505
2	Nose weight radius	1.77	1.98
3	Center of main spar distance from the leading edge	35.6	35.8
4	Spar trailing edge distance from the leading edge	38.9	43.1
5	Spar flange thickness	1.5	2.2

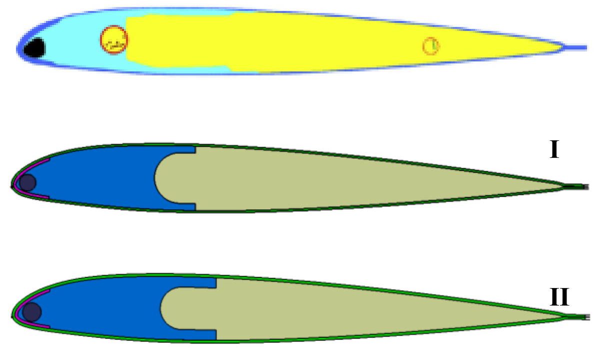

Figure 8. Segmented image of HARTII blade cross-section and comparison with optimization iterations

Campbell diagrams for the resulting blades are shown in Fig. 9 vis-à-vis that of the baseline blade. Only the relevant first six frequencies of the optimized blades are shown in order to keep the diagram tidy. Since the root area has remained unchanged, the lower frequencies have remained almost the same for the resulting blade as it was for the baseline. Reflecting the constraints used, the second lag frequency for blade I is close to 4/rev while for blade II, it is above 4.1/rev. Also, the total weight of the blade I is 2.37kg while that for blade II is 2.59kg which is more than 10% overweight compared to the baseline blade weight of 2.32kg.

Figure 10 shows the 4/rev harmonics of the hub loads of the optimized blades with respect to that of the baseline blade. Both the rotors demonstrate lower values than those for the baseline rotor for all components of the hub load harmonics

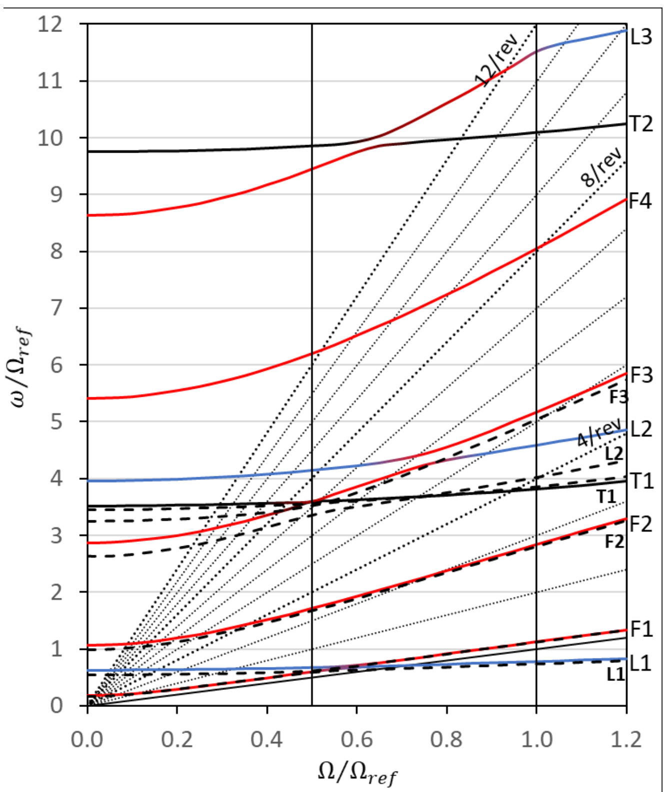

Figure 9. Campbell diagram for the optimized blade (dashed) vs the baseline blade (solid). Blade I case is on the left and Blade II on the right

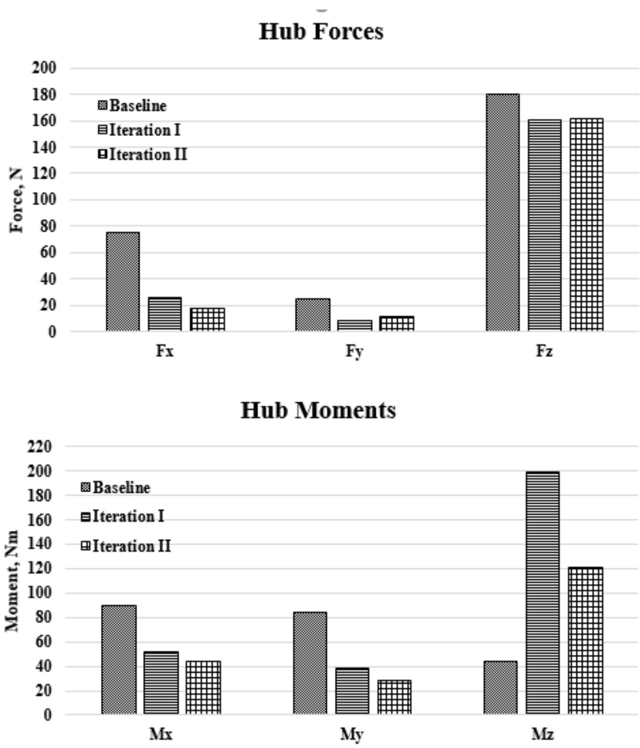

Figure 10. Hub forces and moments for blades I & II compared with the baseline case

except for Mz, which could be attributed to the proximity of the second lag frequency of the blade to 4/rev. Because of the high Mz, the vibration index for blade I comes to 1.02 while that for blade II is 0.87. Blade II has met its goal but with a high mass penalty. On the other hand, since blade I is still within its mass limits, there is potential to utilize lumped masses to adjust its second lag frequency and better its vibratory characteristics.

Vibration reduction with lumped masses

In this step, an optimization exercise was carried out with blade I whereby only the magnitudes of the lumped masses at the tip and at 0.46R (anti-node) are treated as design variables with the constraint being offsetting of the second lag away from 4/rev as much as possible. This exercise resulted in values of 0.009kg for the tip and 0.035kg for the anti-node location. 0.035kg was the upper bound prescribed and it is understandable that the optimizer chose the maximum allowable mass for the anti-node to lower the second lag frequency while tip mass magnitude chosen was negligible as it had minimal influence on the second lag. The lumped masses together add up to 0.044kg which is close to 2% of the mass of the blade. Overall, the mass of blade I is above the baseline by about 4% which is still within the limits prescribed. The resulting Campbell diagram and the hub loads are shown along with the results of the next section.

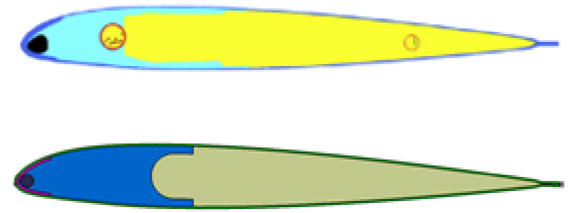

Figure 11. Segmented image of HARTII blade cross-section and comparison with optimization iterations

Table 3. Dimensions of the inner structure

	Design variable	Iter III (mm), (kg)
1	Skin thickness	0.42
2	Nose weight radius	1.42
3	Center of main spar distance from the leading edge	35.5
4	Spar trailing edge distance from the leading edge	39.63
5	Spar flange thickness	1.72
6	Tip mass (kg)	0.0027
7	Anti-node mass (kg)	0.0053

Targeting lower vibratory loads directly

In the final step, all the 7 design variables were taken with the objective of reducing the hub vibrations directly without explicitly constraining the frequencies. The CG-SC and CG-AC offsets and the tip flap deflection were however constrained to be within limits. The resulting inner structure profiles and values of the variables are shown in Fig. 11 and Table 3 respectively. The mass of the blade III comes to about 2.35kg which is slightly higher than that of the baseline. Campbell diagrams for blade III and for the case of blade I with lumped masses are shown in Fig. 12. For the case of blade III, it is seen that the second lag frequency is quite close to the 4/rev. The first torsion frequency is also close to 4/rev but has maintained the minimum offset of 0.1/rev. For the blade I, addition of lumped mass has lowered the second lag frequency slightly to below 4/rev but the magnitude of the mass was not sufficient to offset it by 0.1/rev. A higher reduction may be achieved by increasing the lumped mass slightly.

Figure 13 shows the 4/rev harmonics of the hub loads for these two blade variants. Blade III shows lower hub load harmonics than the baseline blade except for Mz because of the proximity of second lag frequency to 4/rev. Vibration

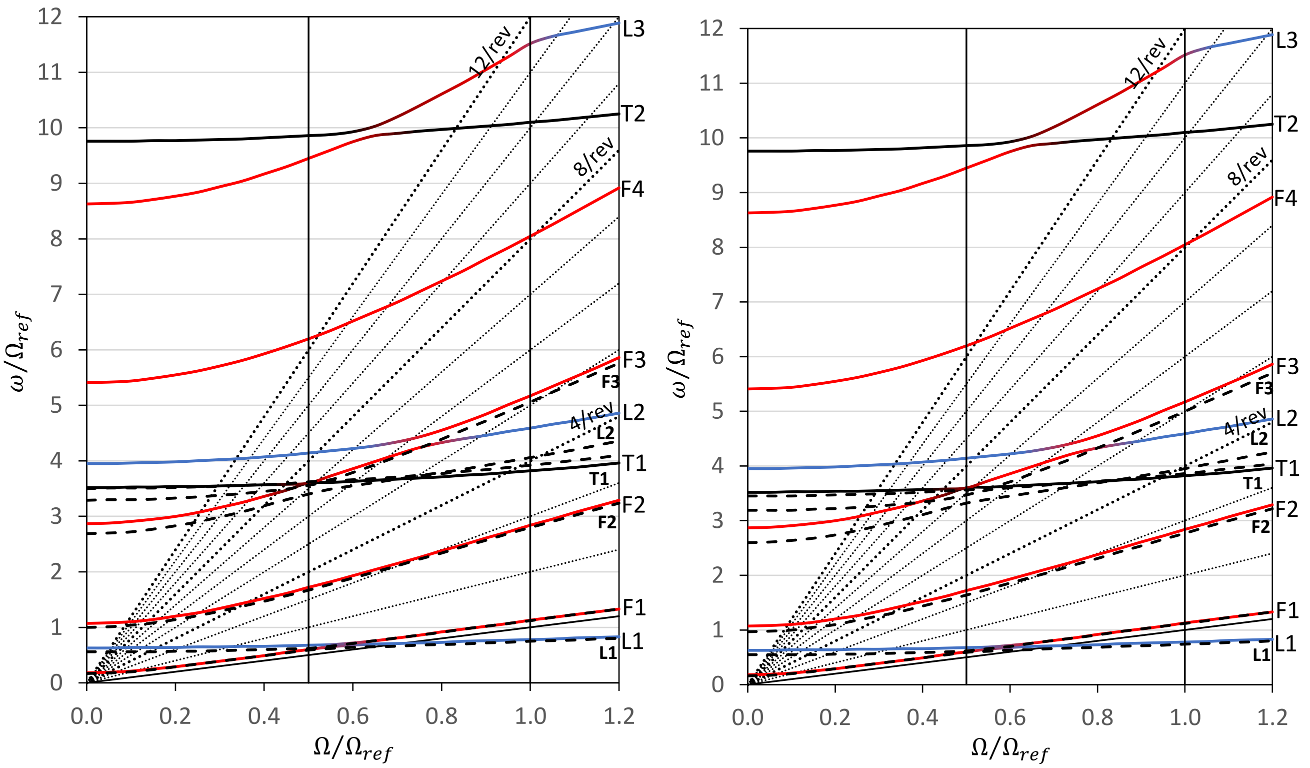

Figure 12. Campbell diagram for the optimized blade (dashed) vs the baseline blade (solid). Blade III case is on the left and Blade I with lumped masses on the right

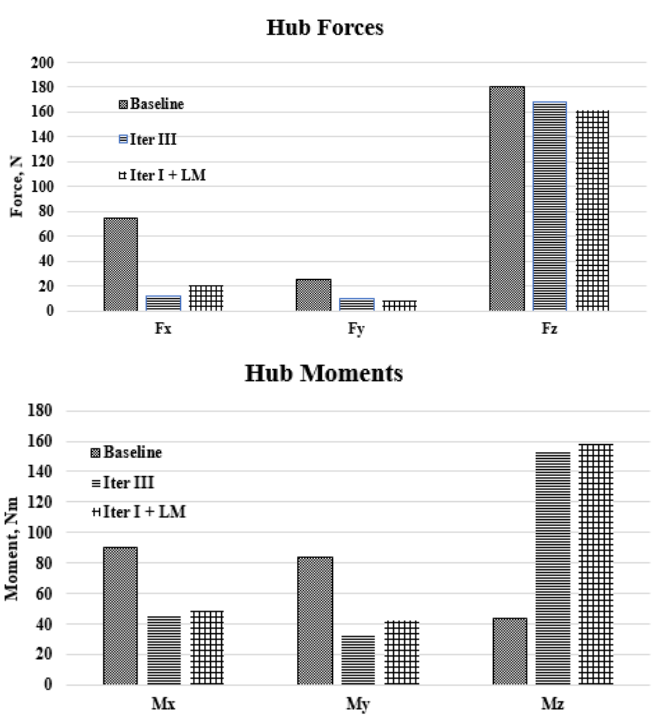

Figure 13. Hub forces and moments for blade III & blade I with lumped masses compared with the baseline case

index for this blade is 0.95 in spite of high Mz. For blade I, the addition of lumped mass has decreased Mz bringing down the vibration index to 0.95.

Tables 4 and 5 give a summary of the constraints and the vibration index for all the blade cases considered. It is seen that while blade II gives the least vibration index (13% reduction), it also comes at the cost of a mass penalty of over 10%. Blade III gives the least vibration index (5% reduction) while also keeping the increases in mass and the flap tip deflection to a minimum. The fact that Blade III and Blade I+LM give similar vibration indices but with different magnitudes of lumped masses goes to show that the design problem is non-convex and advanced methods to find the global minimum are required. A major downside of the obtained results has been the proximity of the second lag frequency to 4/rev for all the blades. This could cause resonance conditions and so is not acceptable in rotor blade design. With the chosen design variables, it has proven to be difficult to obtain as much stiffness in the lead-lag direction as the baseline blade in order to place the lag frequency away from the resonance value.

Table 4. Summary of blade properties for all blades

	Baseline	I	II	III
es (CG-SC)	-0.0045	-0.0048	-0.0059	-0.0056
e0 (SC-1/4c)	0.0055	0.0082	0.0071	0.0082
es+e0 (CG-1/4c)	0.001	0.0034	0.0012	0.0026
m(kg/m)	0.95	0.988	1.118	0.967
Blade mass (kg)	2.32	2.37	2.59	2.35

Table 5. Constraints summary for all blades

	Baseline	I	I+LM	II	III
F1	1.125	1.123	1.123	1.118	1.123
F2	2.839	2.803	2.773	2.792	2.799
F3	5.171	5.036	5.002	5.018	5.063
L1	0.782	0.7405	0.739	0.726	0.745
L2	4.592	4.020	3.953	4.106	4.056
T1	3.810	3.864	3.862	3.735	3.901
z	0.017	0.027	0.024	0.023	0.017
VI	1.0	1.02	0.95	0.87	0.95

CONCLUDING REMARKS

A surrogate-model based optimization procedure with minimal user interaction has been created for the automated design chain of a rotor blade. The framework works well with smooth flow between components. While the framework has been setup, minimal conditions need to be met for the framework to output a truly optimized result. For example, a certain minimum number of sampling points which is problem-dependent are required for setting up a reliable surrogate model. All the relevant design variables need to be considered for achieving realistic designs. In the current work, composite fiber orientations which affect the stiffness properties have not been taken into account. Empirical relations between the design variables to reduce instances of run-time software crashes need to be worked out. Similarly, sufficient constraints need to be defined for a holistic design while at the same time it needs to be ensured that the problem is not over-constrained which could result in no solution. Significant potential exists to reduce hub vibratory loads generated by the blade through careful blade design making use of the simple techniques before resorting to advanced concepts like higher harmonic control. There are multiple areas where the framework could be worked on to make it more robust. The outlook for future includes adapting the framework to the case of rotor blades with non-rectangular planforms which will be an order of difficulty higher with a much larger design space.

Author contact: Rohin Majeti rohin.majeti@dlr.de

REFERENCES

1. Bailly, J., and Bailly D., “Multifidelity Aerodynamic Optimization of a Helicopter Rotor Blade,” *AIAA Journal*, Aug. 2019, Vol. 57, (8), pp. 3132-44. DOI: 10.2514/1.J056513.

2. Fanjoy, D., and Crossley, W. A., “Aerodynamic Shape Design for Rotor Airfoils via Genetic Algorithm,” *Journal of the American Helicopter Society,* Vol. 43, (3), July 1998, pp. 263–270. DOI: 10.4050/JAHS.43.263.

3. Volovoi, V., Li, L., Ku, J., Hodges, D. H., “Multi-Level Structural Optimization of Composite Rotor Blades”. *46th AIAA/ASME/ASCE/AHS/ASC Structures, Structural Dynamics and Materials Conference*, AIAA, Austin, Texas, Apr. 2005, pp. 1–7. DOI: 10.2514/6.2005-2282.

4. Chopra, I., “Design and Analysis Trends of Helicopter Rotor Systems,” *Sadhana,* Vol. 19, June 1994, pp. 427–466. DOI: 10.1007/BF02812163.

5. Blackwell, R. H., "Blade Design for Reduced Helicopter Vibration." *Journal of the American Helicopter Society*, Vol. 28 (3), July 1983, pp. 33-41. DOI: 10.4050/JAHS.28.33

6. Peters, D. A., Rossow, M. P., Korn, A., and Ko, T., "Design of Helicopter Rotor blades for Optimum Dynamic Characteristics." *Computers & Mathematics with Applications,* Vol. 12, (1), Jan. 1986, pp. 85-109. DOI: 10.1016/0898-1221(86)90089-1.

7. Ganguli, R., “Survey of Recent Developments in Rotorcraft Design Optimization,” *Journal of Aircraft*, Vol. 41, (3), May 2004, pp. 493-510. DOI: 10.2514/1.58.

8. Murugan, M. S., Ganguli, R., and Harursampath. D., "Surrogate Based Design Optimisation of Composite Aerofoil Cross-section for Helicopter Vibration Reduction,” *The Aeronautical Journal,* Vol. 116, (1181), July 2012, pp. 709-725. DOI: 10.1017/S0001924000007181.

9. Tian, S., Tao, F., Du, H., Yu, W., Lim, J. W., Haehnel, R.B., Wenren, Y. and Allen, L.D., “Structural Design Optimization of Composite Rotor Blades with Strength Considerations,” In *AIAA SCITECH 2022 Forum* (p. 2454). 10.2514/6.2022-2454

10. Li, L., Volovoi, V. V., and Hodges, D.H., “Cross-Sectional Design of Composite Rotor Blades,” *Journal of the American Helicopter Society*, Vol. 53, (3), July 2008, pp. 240-251. DOI: 10.4050/JAHS.53.240

11. Volovoi, V. V., Yoon, S., Lee, C.-Y., and Hodges, D. H., “Structural optimization of composite rotor blades,” in Proceedings of the 45th AIAA/ASME/ASCE/AHS/ASC Structures, Structural Dynamics, and Materials Conference, (Palm Springs, California), Apr. 2004. DOI: 10.2514/6.2004-1837.
12. Lee, J., and Hajela, P., “Parallel Genetic Algorithm Implementation in Multidisciplinary Rotor Blade Design,” *Journal of Aircraft*, Vol. 33, No. 5, Sep. 1996, pp. 962–969. DOI: 10.2514/3.47042.
13. Visweswaraiah, S. B., Ghiasi, H., Pasini, D., Lessard, L., “Multi-objective Optimization of a Composite Rotor Blade Cross-section,” *Composites Structures,* Vol. 96, Feb. 2013, pp. 75-81. DOI: 10.1016/j.compstruct.2012.09.031
14. Glaz, B., Friedmann, P. P., and Li, L., “Surrogate based optimization of helicopter rotor blades for vibration reduction in forward flight,” *Structural and Multidisciplinary Optimization* Vol. 35, (4), June 2008, pp. 341-363. DOI: 10.1007/s00158-007-0137-z.
15. Collins, K., Bain, J., Sankar, L., Egolf, T. A., Janakiram, R. D., Brentner, K., and Lopes, L., “Pareto Frontier Method for Multi-Disciplinary Optimization of Helicopter Rotors,” Proceedings of the AHS Specialists’ Conference on Aeromechanics, San Francisco, CA, USA, Jan. 2008.
16. Lee, D., Kang, Y., Kim, D. H., and Yee, K., “Improved Surrogate-based Design Optimization of Composite Rotor Blades,” *AIAA AVIATION Forum*, Chicago, IL, July 2022. DOI: 10.2514/6.2022-3360
17. Wilke, G., “A Numerical Optimization Framework for Rotor Airfoil Design”, 48th European Rotorcraft Forum, Winterthur, Switzerland, Sept. 2022.
18. Wilke, G., “Quieter and Greener rotorcraft: concurrent aerodynamic and acoustic optimization,” *CEAS Aeronautical Journal,* Vol. 12, (3), April 2021, pp. 495-508. DOI: 10.1007/s13272-021-00513-x.
19. Pritchard, J. I., Adelman, H. M., Walsh, J. L., & Wilbur, M. L., “Optimizing tuning masses for helicopter rotor blade vibration reduction and comparison with test data,” *Journal of Aircraft*, Vol. 30, (6), Nov. 1993, pp. 906-910. DOI: 10.2514/3.46433.
20. van de Kamp, B., and Wilke, G., “Automation of Structural Cross-Sectional Rotor Blade Modelling for Aeromechanical Rotor Blade Optimization,” 44th European Rotorcraft Forum, Delft, Netherlands, Sept. 2018.
21. van der Wall, B. G., Lim, J. W., Smith, M. J., Jung, S. N., Bailly, J., Baeder, J. D., & Boyd, D. D., "The HART II International Workshop: An Assessment of the State-of-the-Art in Comprehensive Code Prediction." *CEAS Aeronautical Journal,* Vol. 4, July 2013, pp. 223-252. DOI: 10.1007/s13272-013-0077-9.
22. Nagel, B., Böhnke, D., Gollnick, V., Schmollgruber, P., Rizzi, A., La Rocca, G., and Alonso, J. J., “Communication in Aircraft Design: Can We Establish a Common Language?” ICAS, 28th International Congress of the Aeronautical Sciences, Brisbane, Australia, Sept. 2012.
23. M. D. McKay, R. J. Beckman, and W. J. Conover. “A Comparison of Three Methods for Selecting Values of Input Variables in the Analysis of Output from a Computer Code,”. *Technometrics*, Vol. 21, (2), pp. 239–245, May 1979. DOI: 10.1080/00401706.2000.10485979.
24. Sakata, S., F. Ashida, and M. Zako. "Structural optimization using Kriging approximation." *Computer methods in applied mechanics and engineering*, Vol. 192, (7-8), Feb. 2003, pp. 923-939. DOI: 10.1016/S0045-7825(02)00617-5.
25. Leishman, J. G., *Principles of Helicopter Aerodynamics*, Cambridge University Press, New York, NY, 2000, Chapter 5.
26. Gürdal, Z., Haftka, R.T., and Hajela, P., *Design and optimization of laminated composite materials*, John Wiley & Sons, New York, NY, 1999.
27. Eberhart, R. C., Shi, Y., “Particle swarm optimization: developments, applications and resources,” Proceedings of the Congress on Evolutionary Computation (IEEE Cat. No. 01TH8546), IEEE, Seoul, South Korea, May 2001, pp. 81–86. DOI:10.1109/CEC.2001.934374.